NASA TECHNICAL NOTE

NASA TN D-4867

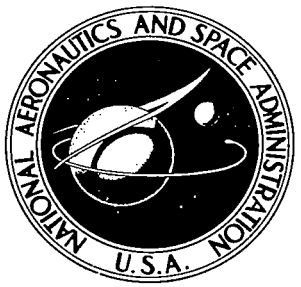

C.1

LOAN COPY: RE
AFWL (WLI
KIRTLAND AFB,

TECH LIBRARY KAFB, NM
0131601

NASA TN D-4867

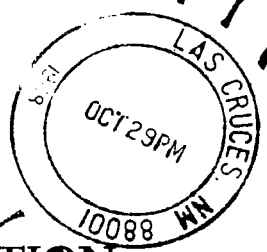

DESIGN AND PRELIMINARY OPERATION OF THE LEWIS MAGNETOHYDRODYNAMIC GENERATOR FACILITY

by Lester D. Nichols, James L. Morgan, Lawrence A. Nagy, Joseph M. Lamberti, and Robert A. Ellson

Lewis Research Center
Cleveland, Ohio

NATIONAL AERONAUTICS AND SPACE ADMINISTRATION • WASHINGTON, D. C. • OCTOBER 1968

TECH LIBRARY KAFB, NM
0131601

DESIGN AND PRELIMINARY OPERATION OF THE LEWIS MAGNETOHYDRODYNAMIC GENERATOR FACILITY

By Lester D. Nichols, James L. Morgan, Lawrence A. Nagy, Joseph M. Lamberti, and Robert A. Ellson

Lewis Research Center
Cleveland, Ohio

NATIONAL AERONAUTICS AND SPACE ADMINISTRATION

For sale by the Clearinghouse for Federal Scientific and Technical Information
Springfield, Virginia 22151 – CFSTI price $3.00

ABSTRACT

The NASA-Lewis closed-loop facility has been designed to study the feasibility of an argon-cesium MHD generator. The construction details, performance, and some preliminary research data are discussed. The facility has operated for several hours at the following conditions: argon flow rate, 1.8 kg/sec; Mach number, 0.3 to 0.5; stagnation temperature, 2100 K. Thus far, open-circuit voltages equal to 60 percent of theoretical value (at 50 V) were measured. In addition short-circuit currents up to 0.8 A (per electrode pair) were measured. This is in agreement with the calculated value using equilibrium conductivity. Leakage currents prevented better performance.

DESIGN AND PRELIMINARY OPERATION OF THE LEWIS MAGNETOHYDRODYNAMIC GENERATOR FACILITY

by Lester D. Nichols, James L. Morgan, Lawrence A. Nagy, Joseph M. Lamberti, and Robert A. Ellson

Lewis Research Center

SUMMARY

The NASA-Lewis closed-loop facility has been designed to study the feasibility of an argon-cesium MHD generator. The construction details, performance, and some preliminary research data are discussed. The loop contains a compressor, regenerative heat exchanger, heater, supersonic nozzle, MHD channel, and two additional heat exchangers. Several auxiliary systems augment the loop operation, for example, cesium-injection system, vacuum pumps, dryer, etc.

The operating characteristics that have been achieved to date in the NASA facility are maximum gas stagnation temperature, 2100 K; maximum gas stagnation pressure in duct, 2 atmospheres absolute (2.02×10^5 N/m^2); maximum gas stagnation pressure in heater, 4 atmospheres absolute (4.04×10^5 N/m^2); argon mass flow rate, 1.8 kilograms per second; Mach number, 0.3 to 0.5; maximum magnetic induction, 2 teslas; heater power, 1.5 megawatts.

Thus far, open-circuit voltages of 50 volts (60 percent of theoretical) were measured. In addition, short-circuit currents up to 0.8 ampere per electrode pair were recorded. This is in agreement with the calculated value using equilibrium electrical conductivity. Leakage currents prevented better performance.

INTRODUCTION

The future of low-temperature (below 2000 K) MHD power generation rests on the premise that nonequilibrium ionization will increase the conductivity of the gas flowing through the MHD duct sufficiently to make this mode of power generation feasible. The NASA-Lewis closed-loop facility is designed to study MHD power-generation problems with an argon-cesium working fluid. Presently, these problems include plasma nonuni-

TABLE I. - CLOSED CYCLE MHD INSTALLATIONS

Location		Gas	Seeding	Conversion duct dimensions, cm		Gas temperature, K	Gas operating pressure, 10^5 N/m^2	Mass flow rate, g/sec	Gas velocity, m/sec	Mach number	Seed concentration, percent	Magnetic field, T
Country	Institution			Cross section, cm^2	Length, cm							
USA	NASA Lewis	Argon	Cesium	6.3 by 19	69	2200	{0.15 static 4.8 total}	2420	1300	3.0	0.03 to 0.3	2.0
	Westinghouse	Helium		5.5 by 7	40	1840	1	15	130	0.1	0.1	1.7
	Allied Division General Motors	Helium		2 by 3	45	1700	1	[a]17.5	1045	0.51 to 0.57	0.3 to 1	2
	Avco-Everett	Argon		Disk	-----	1800 to 2000	----------	----------	----------	----------	0.1	-----
	Avco-Everett	Argon		Disk[b]	-----	1500 to 4000	0.5 to 1	10 000	1300	2	0.1 to 0.3	3
	MIT	Helium		10 to 15 by 3.8	46	2000	5	400	3500	2 to 2.5	0.2	1.4
	General Electric Space Sciences Laboratory	Argon	----------	[c]5 by 5	28	5100	0.4	146	----------	1.28	----------	2.6
		Argon	Cesium	1.25 to 1.84 by 5	25	1500	1	100	400	0.6	0.02	2.25
		Neon, helium, or argon	Cesium	[d]16 by 10	100	1500 to 2000	4 to 20	10^3 to 5×10^4	1000 to 2000	[e]~1.5	0 to 0.1	2
United Kingdom	International Research and Developed (Mk. II)	Helium	Cesium	1.5 by 6	55	1300 to 2200	0.3 to 1	6 to 12	200 to 1800	<0.1 to 0.8	0.01 to 1.8	2.2
	Atomic Energy Research Establishment	Argon or helium	Potassium or cesium	3 by 1.5	20	1500	1 to 6	[f]≥300 and ≥30	----------	0.8	0.1 to 1.0	1.6
France	Commissariat a l'Energie Atomique	Helium	Cesium	5.5	42	1800	<2.5	150	1600	0.3 to 2	<1	2
Japan	Japan Atomic Energy Research Institute	Argon	Potassium	1.5 by 8	22.5	1900 to 2200	1	53 to 33	150 to 130	0.19 to 0.15	1	2
Italy	CNEN Frascati	Helium	Cesium	5 by 3	22	2000	6	400	----------	0.6	----------	4
Federal Republic of Germany	Institut für Plasmaphysik Garching	Argon	Potassium	2 by 2.5	20.5	2000	0.3 to 0.5	100	650	0.7	0.04 to 2.9	<3.5
	Kernforschungsanlage Julich	Argon	Cesium	5 by 10	50	1800	1 to 8	4000	----------	0.9	----------	1.8
USSR	I. A. E. Kurchatov Moscow	Argon	Cesium	Disk[g]	-----	1300	<10	<1000	----------	1.8 to 3	0.01 to 0.1	4

[a]Helium.
[b]Tailored interface shock tube.
[c]Shock tube.
[d]Diverging.
[e]Entrance.
[f]Argon and helium, respectively.
[g]Minimum radius 22 cm, maximum 60 cm.

formities and instabilities, shorting of the generated voltages either through the plasma or the structural material, and the problems associated with starting the nonequilibrium ionization.

A summary of the important design parameters of the Lewis MHD generator facility in comparison with other facilities is presented in table I (see ref. 1). The Lewis generator cross-sectional area is large compared with those of other facilities currently being used or constructed. The large area was chosen to reduce wall friction and boundary-layer effects, to generate high voltages ($v = uBd$) in the conducting fluid, and to provide a large volume to reduce energy loss from the electrons to the walls by radiation and conduction. A steady-state experiment was chosen so as to simulate better the conditions under which the generator must perform. The theoretical performance of the Lewis (Brayton cycle) MHD generator was evaluated by Heighway and Nichols (ref. 2). In that analysis the cycle efficiency and output-power density were optimized with respect to load voltage, seed fraction, and operating pressure.

The MHD duct (1.95 m by 6.35 cm by 19 cm) contains 28 pairs of rectangular thoriated tungsten electrodes on 2.54-centimeter centers. These electrodes are located in the center third of the duct length. This electrode region is in the center of a 0.914-meter magnetic-field region.

The selection of compatible materials to withstand 2200 K is the most difficult engineering problem. Accompanying the description of the facility is a discussion of the loop performance and some preliminary experimental data. These data were taken during five runs. Between the first three and the last two runs certain modifications were made to the loop. The effects of these modifications are discussed.

FACILITY

General Description

Figure 1 shows the loop schematic, and figure 2 shows an artist's conception of the high-temperature components located in the test cell. The gas leaving the compressor is preheated in a parallel flow regenerative heat exchanger (reheater) before entering the graphite resistance heater. Cesium is injected into the loop at the entrance to the nozzle. On leaving the heater via the nozzle the hot gas enters the MHD channel, expands in the diffuser, and enters the shell side of the reheater. From this point conventional equipment cools, dries, and filters the gas as it flows toward the compressor. The flow-control valve loads the compressor. The bypass valve permits a wide variation of mass flow through the heater.

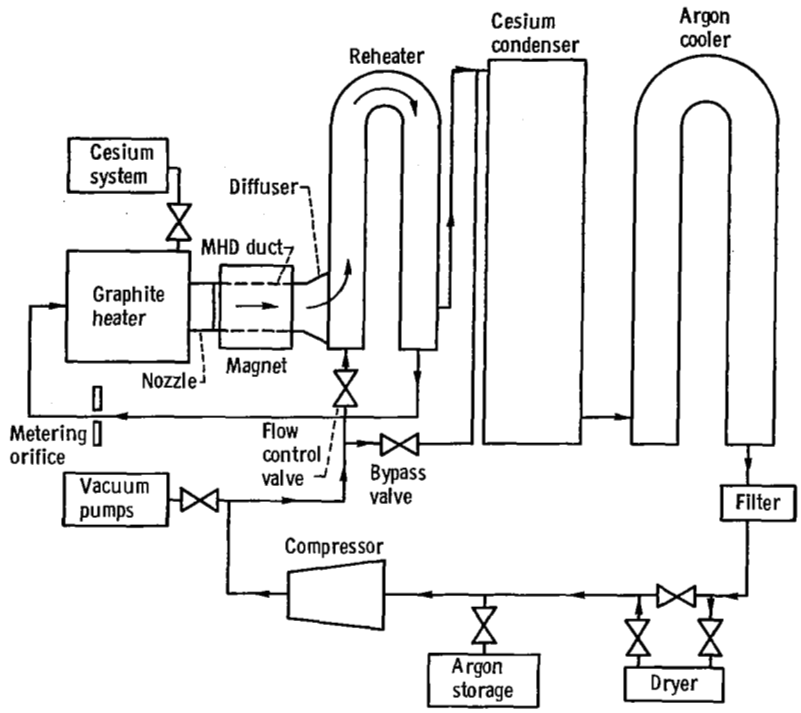

Figure 1. - Loop schematic.

Heater

Structure. - The heater shown in figure 2 has several main parts: the outer water-cooled stainless-steel shell, the lining of high-density castable refractory cement, a set of four graphite heater elements surrounded by magnesium oxide bricks, and an inlet molybdenum flow distributor (not shown in fig. 2). The flow distributor (fig. 3) effectively distributes the incoming gas through the vertical slots in the graphite heater element which is shown in figure 4. The dimensions of the heater elements are 1.17 by 1.04 by 0.228 meter and the slots provide a surface area of 16.2 square meters per element for heat transfer. Figure 4 also shows how the heater elements and the magnesium oxide brick are assembled in a molybdenum pan and installed in the heater cavity. The insulating brick has been cut back on the vertical sides. The resulting local gas cooling prevents formation of hot spots. Previously, local hot spots in these areas were sites for arcing. Originally, a tantalum frame supported the brick. However, during the curing of the castable refractory, water vapor was librated. The tantalum decomposed the water, combined with the oxygen, and became embrittled from the resulting hydrogen. The present self-supporting structure is satisfactory. After several hundred hours of operation only the downstream heater element shows signs of wear: its surface is rough.

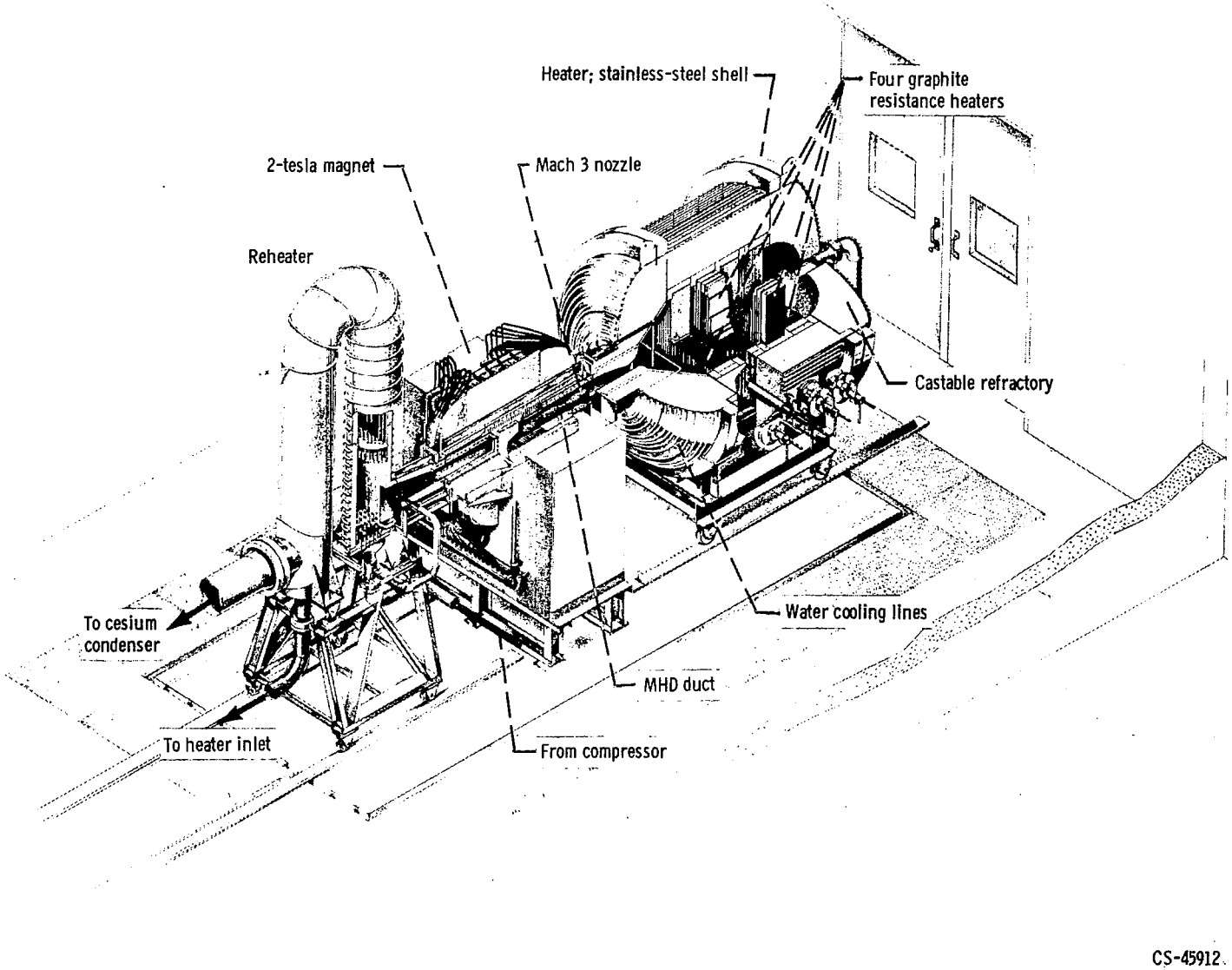

Figure 2. - Bedplate showing heater, nozzle MHD duct, magnet, and reheater. The flow distributor at the heater inlet is not shown.

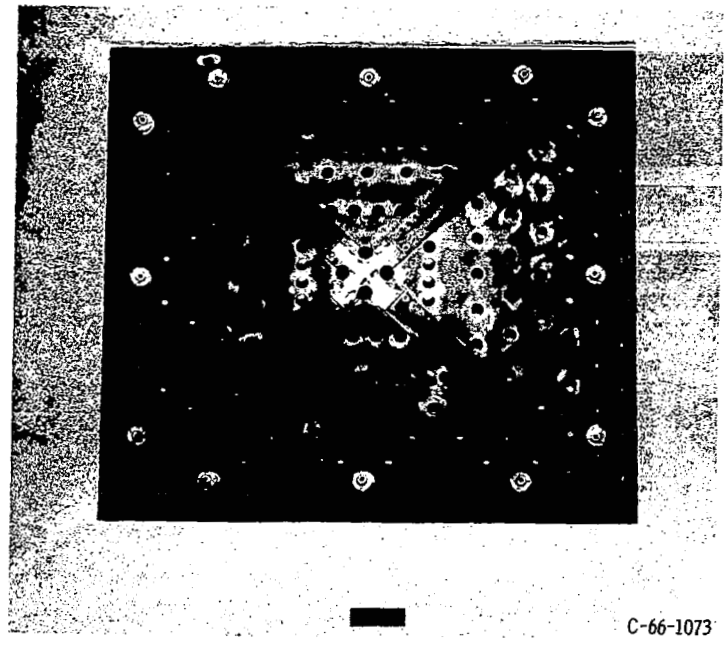

Figure 3. - Heater front end bell showing inlet molybdenum flow distributor.

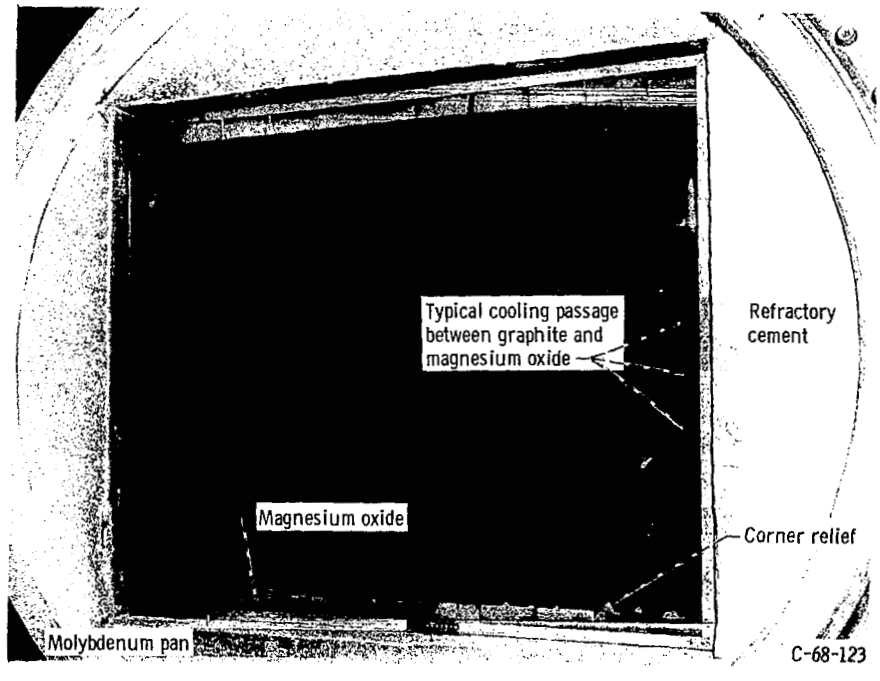

Figure 4. - Graphite heater element installed on heater.

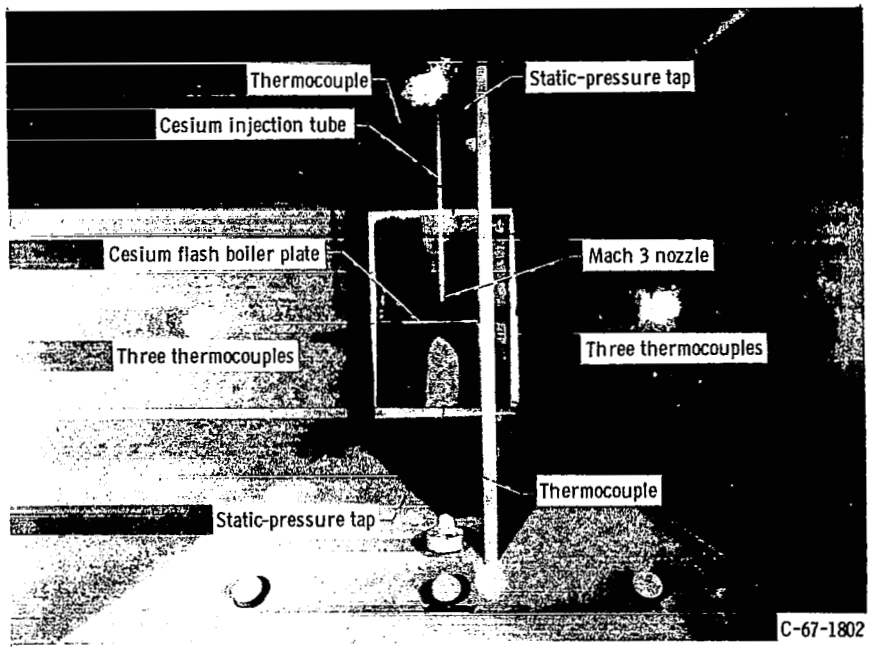

Figure 5. - Heater discharge end bell with flash boiler and nozzle entrance.

Hot gas, leaving the last heater element, enters the heater discharge end bell (the area just upstream of the nozzle) shown in figure 5. Here graphite plates, 2.5 centimeters thick, protect the castable refractory from melting. This refractory is rated at 1900 K. Figure 5 shows the nozzle entrance area, the cesium boiler, and the location of pressure and temperature sensors.

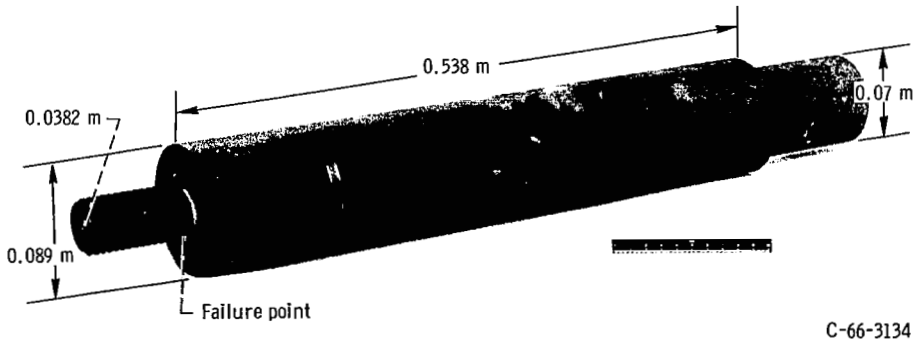

(a) Connector used on runs 1 to 3.

Figure 6. - Graphite power connectors.

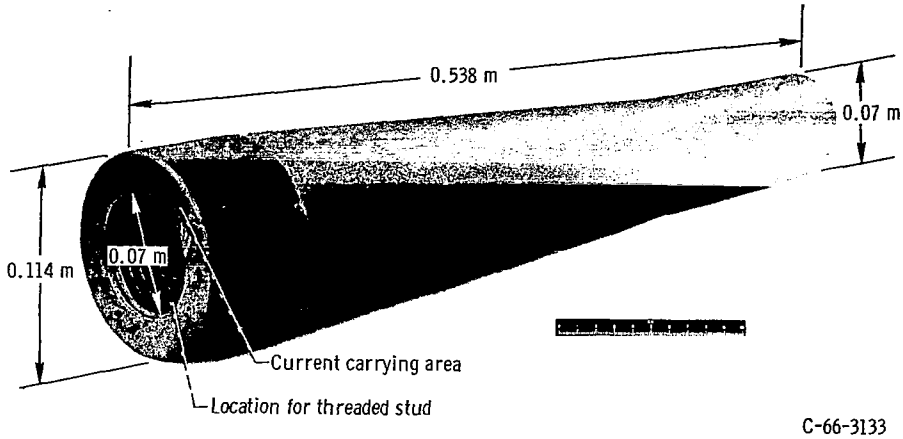

(b) Connector used on runs 4 and 5.

Figure 6. - Concluded.

The graphite power connectors are shown in figure 6. These power connectors to the main heating element required redesign. The early design (fig. 6(a)) failed at the thread relief. The new design (fig. 6(b)) eliminated this stress concentration by replacing the original threaded portion with a separate threaded stud. Several hundred hours of satisfactory operation have been achieved with this design.

Electrical. - The four graphite heater elements raise the temperature of 2.42 kilograms per second of argon from 940 to 2200 K. The heater is rated at 1725 kilovolt-amperes. Figure 7 shows the heater wiring diagram. The three-phase system consists of a 1150-kilovolt-ampere delta-wye transformer which powers three heater elements, forming a balanced delta load. A single-phase 575-kilovolt-ampere transformer powers the remaining heater element. The saturable reactors located in the primary side of each transformer control the power to the load. The phasor diagram shows the relative position of the four voltage phasors for the revised electrical connection. The 1000-ohm resistors fix the potential of Y1 midway between that of X3 and X11. In principle, the electrical connections minimize the potential difference between heaters 2, 3, and 4. With the original connection as shown in figure 7, arcing occurred between heater elements 2 and 3 and 3 and 4 at a power level of 1.1 megawatts during runs 2 and 3. Rewiring the heater, machining the element corners, and recutting the side bricks (see fig. 4) to help prevent hot spots has resulted in the heater operating satisfactorily at a power of 1.5 megawatts during runs 4 and 5. Thus, it was not necessary to power the four elements wired in parallel and thereby eliminate the potentials between them. More detailed heater performance will be discussed in the section Heater Performance.

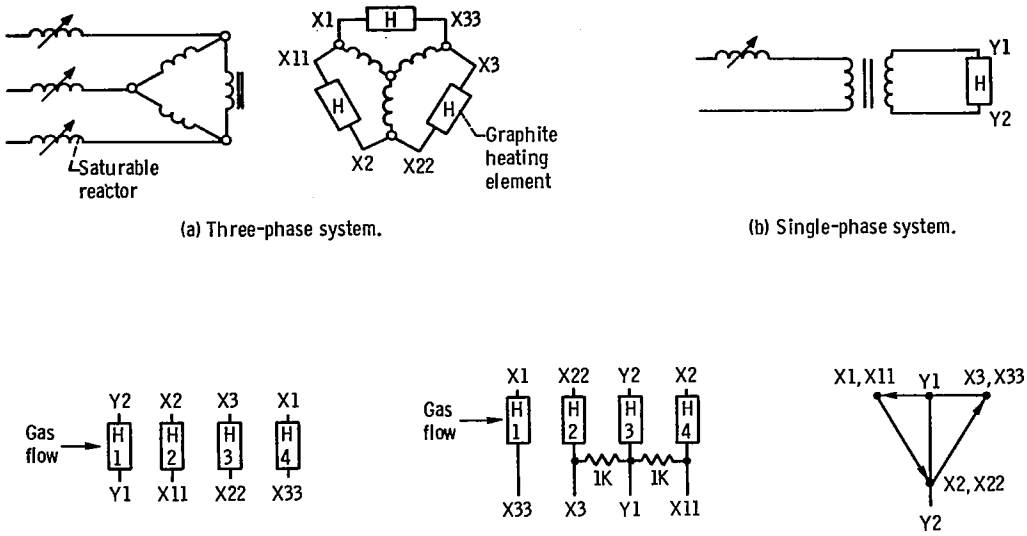

(a) Three-phase system.

(b) Single-phase system.

(c) Original connection (runs 1 to 3).

(d) Revised connection and phasor diagram (runs 4 and 5).

Figure 7. - Heater power system.

Nozzle

The one-dimensional nozzle is designed for a Mach 3 flow. It consists of two contoured graphite blocks with parallel graphite side plates. Initially, the surfaces were coated with plasma-sprayed tungsten (0.75 mm thick). However, at high temperatures, the tungsten coating spalled. This was attributed to the differences in the expansion coefficients of the two materials. In all subsequent tests an unplated nozzle was used. The unplated nozzle showed no signs of wear after several hundred hours of operation. The throat cross-sectional area remained 6.35 by 6.04 square centimeters.

Cesium-Injection System

The schematic of the cesium injection system is shown in figure 8. Provisions are made to heat, purge, evacuate, and vent the system. The mass flow rate can be regulated from 1 to 20 grams per second. Cesium storage volume was 6.82 kilograms.

During a normal operating cycle, the system was heated to a temperature of 338 K. Atmospheric moisture and oxygen were removed from the system by repeatedly charging it with argon and then evacuating the system to 10^{-3} torr. After this is completed, the system is ready for operation. Argon pressure drives the cesium from the reservoir through a set of calibrated orifices. Downstream of the shutoff valve (fig. 8), the liquid

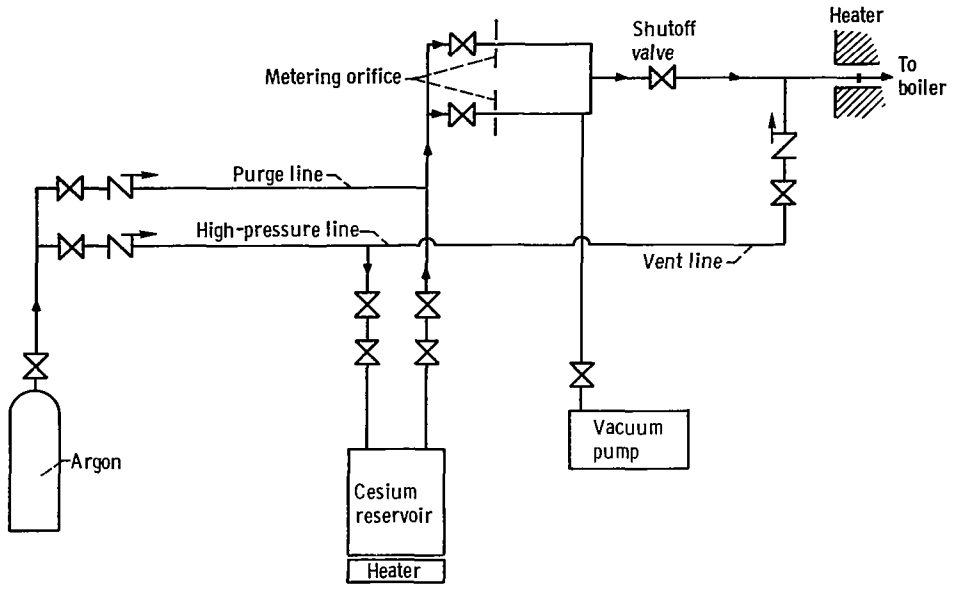

Figure 8. - Cesium injection system schematic. (All lines and valves in contact with cesium are heated to 338 K.)

cesium flows through a 6.1-millimeter-diameter molybdenum tube into a molybdenum cesium flash boiler. Figure 5 shows this cesium flash boiler installed in the heater discharge end bell.

Prior to opening the system, the condensed cesium must be oxidized. The argon in the loop is slowly displaced by a controlled amount of atmospheric (i.e., humid) air. The amount of hydrogen gas generated by the reaction between cesium and the atmospheric air is monitored. The loop was evacuated each time the amount of hydrogen gas reached 4 volume percent of the total loop gas. The cycle was repeated until no hydrogen gas was detected.

MHD Generator

Duct structure. - Two conditions must be satisfied in the generator: (1) insulation resistance between electrode pairs and between each electrode and ground must remain high; (2) the refractory brick, used to line the walls, must be able to withstand the stresses imposed by adverse temperature gradients and varying dynamic loads. The design used for the first set of runs (1 to 3) was changed because of structural failures of the side walls. Figure 9 shows the duct as it was tested in runs 4 and 5. Stainless-steel cooling lines are welded to the inside surfaces of the duct's four stainless-steel sides. In addition to the internal cooling lines, external cooling lines are soldered to the top and bottom skins of the duct. The internal cooling lines are cast in 5 centimeters

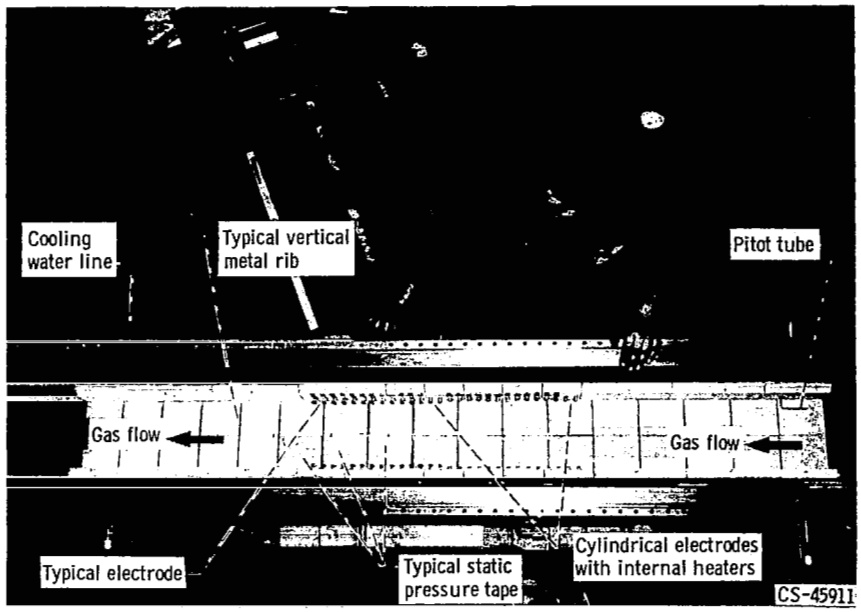

(a) Side view.

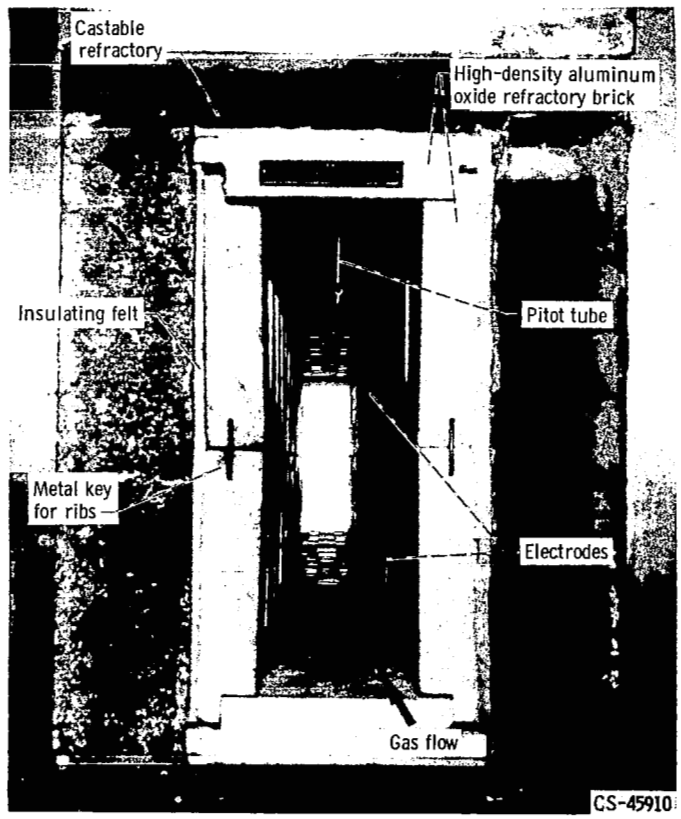

(b) End view.

Figure 9. - MHD duct.

of high-density refractory cement. This, in turn, is protected from the hot gas by high-density (3.1 g/cm^3) alumina brick.

Figure 9(a) shows the location of the electrodes, the Pitot tube, static pressure taps, and the vertical metallic ribs used to support the refractory brick. These ribs are cast into the refractory cement. Figure 9(b) shows the axial key that threads through the ribs and holds the bricks in place. This modification provided adequate support in the center of the duct, but did not hold in place the side-wall bricks near the entrance to the duct. Further modifications are to be made to improve this situation.

Electrodes. - The electrode design used in runs 1 to 3 was a rectangular (8.9 by 1.27 cm^2) 2-percent-thoriated-tungsten plate mounted flush with the wall. For runs 4 and 5 buttons were added to the plate as shown in figure 10. The buttons of the electrode plate penetrate the fluid boundary layer; therefore, the flowing gas can raise the electrode temperature and thus improve its thermionic emission. The buttons located on the first 14 electrodes are 0.61 centimeter high and the rest 1.22 centimeters above the plate (see fig. 9(a)). In this configuration electrode currents up to 0.8 ampere have been measured. In addition, each of the four cylindrical electrodes shown in figure 9(b) contains a separate thermocouple and heater. Improved performance with the heated electrodes was not obtained. Therefore, because satisfactory performance was achieved with the buttons, it was concluded that separately heated electrodes are unnecessary.

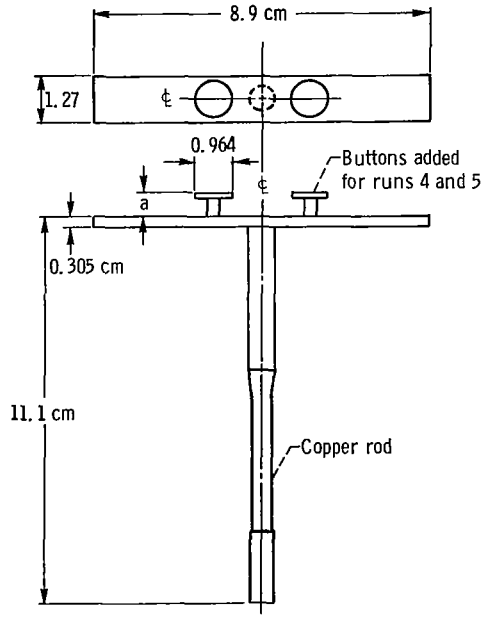

Figure 10. - Typical MHD generator electrode. All material 2 percent thoriated tungsten except where noted. (a = 0.5 cm for electrodes 1 to 14; a = 1.0 cm for electrodes 15 to 28.)

Regenerative Heat Exchanger (Reheater)

A parallel flow regenerative heat exchanger (see figs. 1 and 2, pp. 4 and 5) recovers approximately 35 percent of the fluid stagnation enthalpy. Parallel flow was selected (instead of a counterflow heat exchanger) to keep the heat exchanger tube temperature low. This permitted the tube to be made from nonrefractory materials.

The reheater contains 56 tubes. Each is approximately 6.35 meters long and measures 2.54 centimeters in diameter. The temperatures of both gas streams are within 20 to 30 K of each other as they leave the reheater, which indicates that sufficient surface area is provided for efficient energy transfer. The only unusual design feature is an internal lining of insulating, castable refractory, 2.54 centimeters thick, protecting the outer stainless-steel shell from contact with the hot gases. In addition, seven separate water circuits are used to cool the outer stainless-steel shell. Both the inlet and discharge temperatures and pressures of the two gas streams are measured to evaluate the performance of the reheater.

It was necessary to build a new reheater because several of the tubes were embrittled at high temperatures by contaminants in the gas stream. These contaminants are discussed in a later section. The embrittled tubes eventually failed and bypassed 20 percent of the gas flow.

The failure of the reheater tubes was related to a flow separation that occurred in the MHD duct during the initial duct test. Because the pressure ratio across the nozzle was not matched for either subsonic or supersonic flow, the interim value resulted in the formation of a separated boundary layer in the diffuser. For that reason, the hot gas stream was confined to the center of the duct, and the stream did not expand in the diffuser. Therefore, the stream stagnation energy was concentrated on a small area at the entrance to the reheater. The combination of a high-energy flux on a small area and the presence of contaminants caused the eventual failure.

A horizontal wedge was inserted at the inlet to the existing reheater to retard further deterioration of the embrittled tubes. The wedge increased the recoverable dynamic pressure in the diffuser from 2.54 to 7.62 centimeters mercury (1.0×10^4 N/m^2). This interim alteration made it possible to use the reheater for over 100 hours while a new one was being fabricated.

Several minor modifications were made in the new reheater design. The diffuser, originally an integral part of the reheater, has been separated by a mechanical joint. Furthermore, a single vertical wedge has been installed to deflect the separated flow from the reheater tubes. In addition, the cross-sectional area of the inlet flow passage to the reheater has been increased. The internal tube material was changed from 316 stainless steel to a nickel based alloy (76 nickel, 15.8 chromium, 7.2 iron). This may provide better protection at high temperatures against attack by carbon monoxide,

one of the major contaminants. Also, the thickness of the internal refractory liner was increased from 2.54 to 3.81 centimeters. All modifications were made to improve the structural integrity of the reheater.

High-Temperature Piping

The castable refractory cement lines the piping from the reheater to the cesium condenser (see fig. 1, p. 4). This liner insulates the stainless-steel pipe from the hot gas. During inspection of the pipe leading to the cesium condenser, large areas of bare pipe at an elbow were noted. During a run, the increase in pressure drop across the filter can be correlated with the cesium injection time. It is possible that the cesium reacted with the silica of the high-density refractory cement. Thus, the cement was weakened and the hot flowing gas carried the powdered cement to the filter. Because the heat transfer to the pipe is sufficiently low, this loss in cement does not appear to be serious. Adequate filter capacity must be provided because of the powder in order not to reduce the operation time inordinately.

Cesium Condenser

The condenser is a single-pass, counterflow, gas to mineral oil heat exchanger designed to reduce the gas temperature from a maximum value of 1200 K to 340 K, thus condensing the cesium entrained in the flow stream. A sump is located at the base of the unit. It is considered a hazard to use water as a coolant because large amounts of cesium could deposit in the condenser. If a leak occurred, the hydrogen liberated by the reaction of

$$2Cs_2 + H_2O \rightarrow H_2 + 2Cs_2O$$

might produce an explosive mixture. Mineral oil was chosen as the coolant because it does not react with cesium. A pump circulate 1135 liters per minute (300 gal/ min) of mineral oil through a water-cooled heat exchanger. The hot gas in the condenser flows through 129 tubes, each 8.14 meters long with a diameter of 0.0318 meter.

Argon Cooler

The cooler is a U-shaped, counterflow, water-cooled heat exchanger. To obtain an exit gas temperature of 295 K required at the compressor inlet, a 15-ton (52.9-kilowatt)

chiller extracts the energy from the circulating cooling water. As in the condenser, the warm gas flows inside the 99 tubes. Each tube is 14.4 meters long and has a diameter of 0.0254 meter. The argon cooler serves further to solidify any residual cesium carried through the cesium condenser.

Filter

A filter is located downstream of the argon cooler to remove solid impurities resulting from the high-temperature portions of the loop. The filter element, constructed of woven glass for compatibility with cesium, is the radial fin type. It was not anticipated that cesium would carry over from the argon cooler, and only after one of the runs has cesium been detected in the filter. The filter is designed to remove particles of 10 micrometers and larger and has an area of 9.5 square meters.

Materials present in the filter after a run consist primarily of castable refractory residue, some carbon from the heating elements and other graphite structures, and traces of cesium as noted previously.

Because of the unexpectedly large quantities of castable refractory continually being removed primarily from the reheater and piping, it became evident that filter capacity severely limited running time at the highest temperatures. For this reason the filter capacity has been increased to 46 square meters.

Dryer

All the high-temperature components from the heater to the cesium condenser are lined with a high-density refractory cement. To cure this material, the mechanically and chemically bonded water has to be driven off. A dryer was placed in the loop. A partially closed butterfly valve diverts approximately 5 percent of the flow through the dryer (fig. 1). The amount of water the dryer can hold before it becomes saturated varies directly with the dew point of the entering gas stream. For example, as the stream dew point varied from 242 to 208.6 K, the amount of water that can be absorbed declines from 42.9 to 10.96 kilograms. The dryer loop contains the necessary equipment to reactivate the desiccant. When heated to 605 K the desiccant releases its absorbed water. Dry preheated gases (i.e., first air, then argon) are used in the reactivation.

Compressor

The two-stage, double acting, reciprocating compressor, operating at a suction pressure of 1.14 atmospheres absolute (1.14×10^5 N/m^2), discharges 2.42 kilograms per second of argon at a pressure of 6.8 atmospheres (6.8×10^5 N/m^2) absolute and 450 K. This compressor is designed for nonlubricated operation, having piston rings and shaft seals made from graphite impregnated tetrafluoroethylene. To prevent the leakage of atmospheric air into the loop, all shaft seals are externally pressurized with argon. A 600-kilowatt synchronous motor, operating at 225 rpm drives the compressor.

Argon Storage

Two large skids, each with a capacity of 30 000 standard cubic feet (849 standard m^3) are used to store the argon. They are connected in parallel and pressurized to 150 atmospheres (1.5×10^7 N/m^2). This capacity is sufficient to fill the entire loop approximately 40 times from several torr to 1 atmosphere (1.01×10^5 N/m^2). The argon is also used to provide gas for actuating remote operated valves, for dryer reactivation, and for compressor seal use.

Vacuum Pumps

Two mechanical vacuum pumps evacuate the loop to a pressure of 2 torr. Their oil sumps are equipped with internal water-cooled coils. The entire loop can be evacuated in less than 15 minutes without overheating the oil. This rate is maintained even when the loop is charged with hot gas.

Generator Load Bank

The load bank dissipates the electrical power generated in the MHD generator. Each of the 28 pairs of electrodes is connected to a separate electrically isolated circuit. The load consists of a series of immersion heaters enclosed in a number of water tanks. The load resistance in each circuit can be varied in steps from a fraction of an ohm to several ohms.

Magnet

The magnet is rated at 330 volts and 1500 amperes, direct current. It develops a maximum uniform magnetic field of 2 teslas in the MHD duct. Its pole pieces measure 0.914 by 0.455 meter with a gap of 0.254 meter. The variation of the magnetic-flux density with magnet current is shown in figure 11(a). The variation of the magnetic-field intensity along the test section centerline is shown in figure 11(b). The magnet is protected from high-voltage transients by a circuit consisting of a thyratron controlled ignitron.

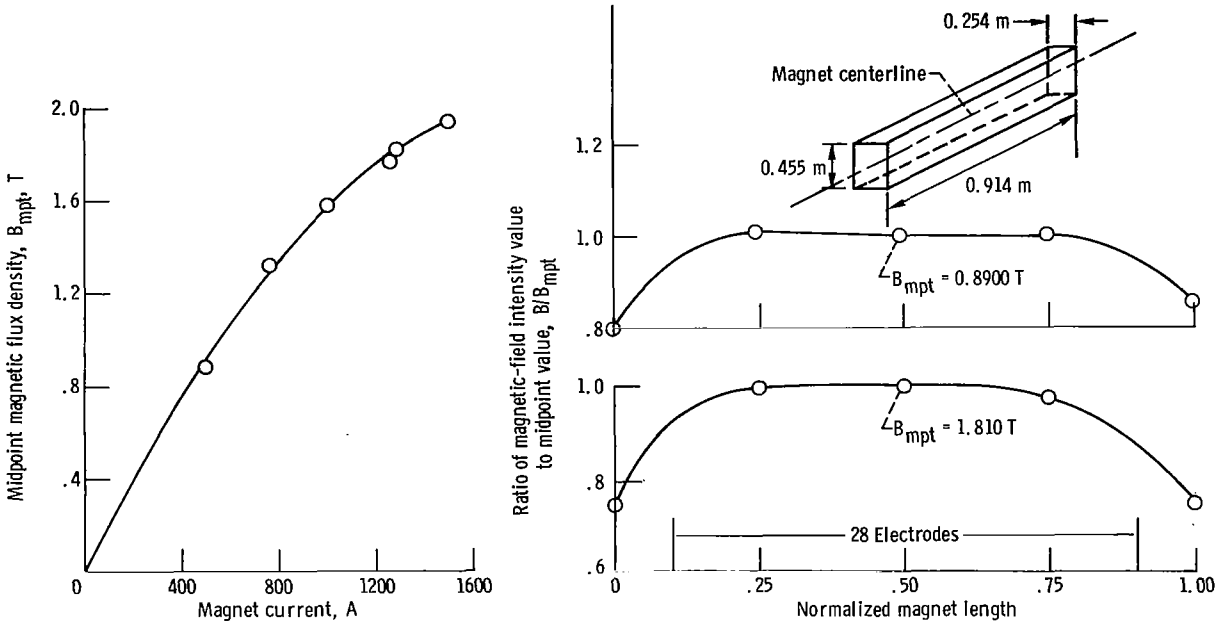

(a) Saturation curve at centerline of magnet. Gap, 0.254 meter.

(b) Ratio of magnetic-field intensity value to midpoint value versus pole piece length for two field strengths. Data taken along magnet centerline.

Figure 11. - Magnet characteristics.

Instrumentation

Approximately 210 thermocouples and 56 pressure gages are monitored each time the loop is operated.

With the exception of the high-temperature thermocouples used in both the heater and the MHD duct, the instrumentation is standard. Figure 12 shows a typical tungsten - tungsten-26-percent rhenium high-temperature thermocouple assembly used in the heater discharge end bell. To measure the power developed in each of the MHD circuits, the 28 currents and voltages are displayed on 56 panel meters.

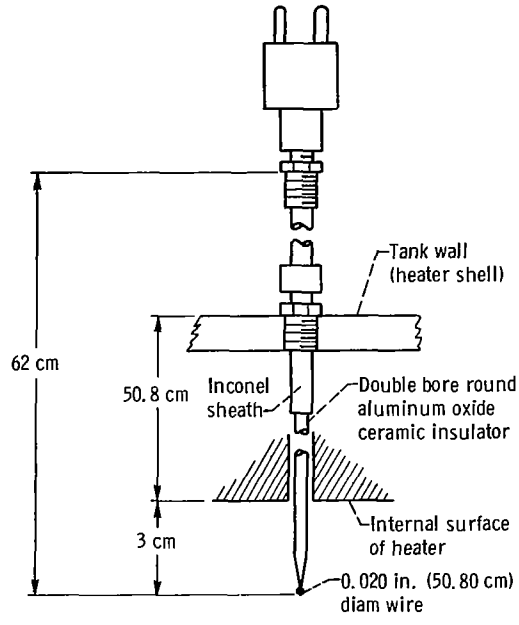

Figure 12. - Typical tungsten - tungsten-26-percent-rhenium thermocouple design used in heater.

The data are recorded by photographing all 56 meters. In addition to this, two 24-point recorders print out selected electrode currents and voltages at a rate of 1 point per second. In future runs the data will be digitized and recorded. The following temperatures and pressures in the MHD duct are measured:

(1) The wall temperature at the inlet and exit of the duct

(2) The surface temperature of the first and last electrode

(3) The total and static pressure near the inlet of the duct

(4) The axial variation of the static pressure at the wall

From these data the free-stream Mach number, the channel friction factor, and the boundary-layer thickness are calculated.

A calibrated orifice, located in the piping between the reheater and the heater, measures the argon mass flow rate (see fig. 1, p. 4).

Emergency Shutdown System

An automatic emergency shutdown system provides personnel and family protection. Certain critical temperature and pressure sensors are wired into a warning and an emergency shutdown circuit. For example, a sudden drop in heater pressure, indicating either a loss of loop gas due to a leak or break in the line, would automatically shut off the heater power. This protects the heater against overheating. The heater is auto-

matically shut down in the event that any of the following occur:

(1) Drop of heater inlet pressure

(2) Loss of cooling water flow to the generator electrode, MHD duct walls, reheater walls, diffuser walls, or cooler

(3) The emergency switch in the cell is turned to the "off" position

The heater and the oil system are automatically shut down, and argon pressure forces the cooling oil in the condenser back into the storage tanks for any of the following conditions:

(1) Overtemperature of the oil in the condenser (flash point, 400 K)

(2) Loss of oil pressure in the condenser

(3) Loss of control power to the oil system and argon loop valves

Because the heater has an enormous thermal capacity, merely stopping the power does not prevent the gas from being heated. The compressor must be stopped to prevent the energy transfer by the hot flowing gas to other parts of the loop. The compressor is controlled by the operator. It is not in the automatic emergency shutdown circuit.

In addition to the above thermal protection a relief valve prevents excessive pressures. Wherever practical, a flashing light, buzzer, etc., was connected to forewarn the operators of impending difficulties.

PRELIMINARY OPERATION RESULTS

Flow Characteristics

Although the loop was designed to operate with a Mach 3 nozzle, actual operation so far has been subsonic. The pressure ratio required to provide supersonic flow has not yet been achieved, because the eroded holes in the reheater tubes bypassed gas intended for the heater. Thus, the nozzle was overexpanded and the flow passed through a shock wave in the nozzle. The resulting Mach number in the generator section varied from 0.2 to 0.5.

As a result of the shock wave in the overexpanded nozzle, flow separation occurred in the nozzle and in part of the MHD duct. Figure 13 shows the static pressure profile in the MHD duct for two different nozzle pressure ratios. The curve for no separation in the generator is typical for a high nozzle-pressure ratio and a Mach number of 0.4 in the channel. The curve for separation in the generator usually occurs at a lower nozzle-pressure ratio. (As a matter of interest, for the fully attached flow the friction factor f was estimated. In a typical run, e.g., run 2,

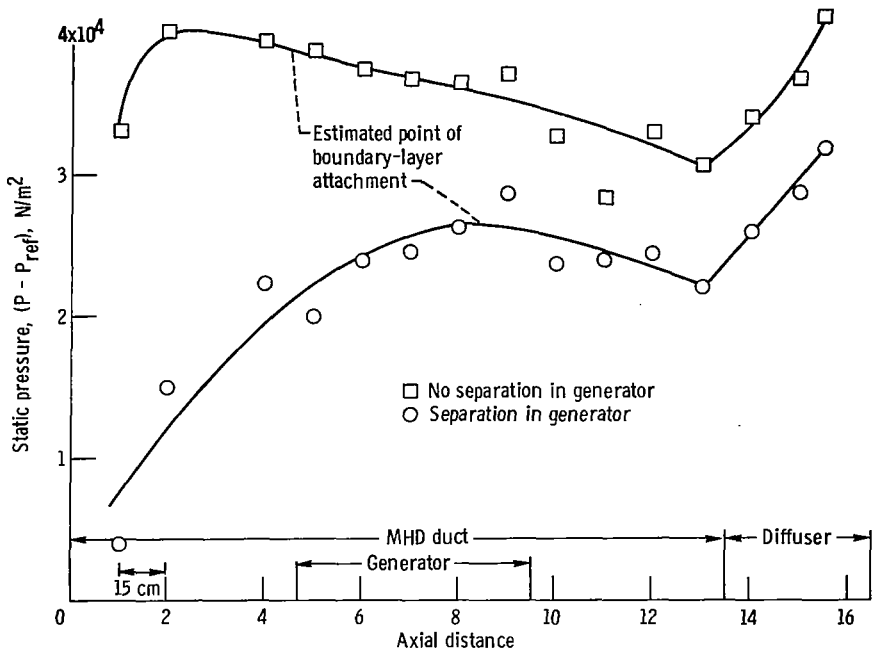

Figure 13. - Static pressure in MHD duct and diffuser. Reference pressure, 1.34×10^5 newtons per square meter.

$$4f \frac{L}{D} = \frac{(-\Delta p)}{\frac{1}{2}\rho u^2} \cong 0.5$$

so that for L/D = 18 then f = 0.007).

Heater Performance

For a typical run, the heater had an efficiency of 85 to 90 percent at an input power of 1 megawatt. When operating with an input power of 1.5 megawatts and a mass flow of 1.27 kilograms per second the inlet and discharge temperatures were 872 and 2100 K, respectively. Because the heater is constructed from 7000 kilograms of insulating refractory cement and 1400 kilograms of graphite, it has a high thermal inertia. Therefore, the time constant for equilibrium is of the order of hours. In figure 14(a) the efficiency, power, and gas stagnation temperature are plotted as a function of running time for run 3. The thermal inertia is evident by comparing the temperature response to the power input time. The efficiency curve also shows the effect of thermal efficiency; that is, the efficiency rises up to the 14th hour at constant heater power input, and drops after the 14th hour as the power input is increased too rapidly. The plot of efficiency

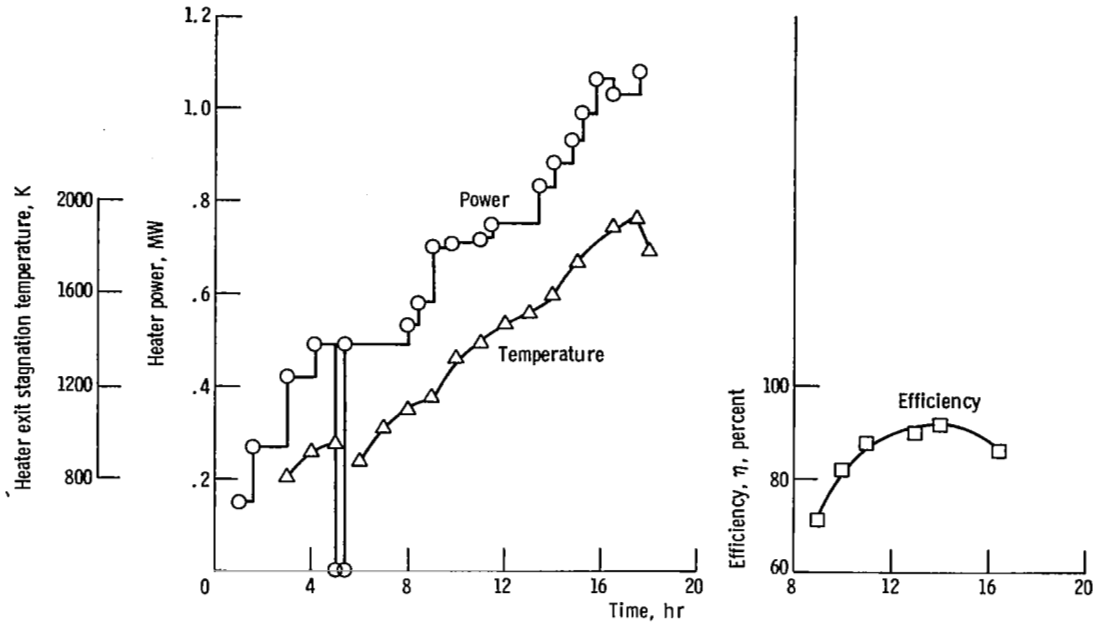

(a) Power, temperature, and efficiency as function of time.

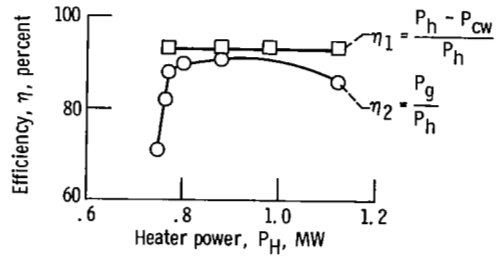

(b) Efficiency as function of power.

Figure 14. - Heater thermal characteristics for run 3.

calculated in two ways as function of heater power appears in figure 14(b). In one case the power transferred to the gas is used; in the other the difference between the power input and the losses is used. The power transferred to the cooling water was directly proportional to the heater power. The difference between the two efficiencies results from the thermal inertia of the heater. The near agreement of the two efficiencies at $\eta \sim 0.90$ indicates that equilibrium (i.e., input power to heater equal to thermal power transferred to the gas) was attained at this power level.

Seed Vaporizer

The seed vaporizer performance can be evaluated from generator voltage measure-

ments. The instant that the cesium vapor appears in the generator, the plasma conductivity increases sufficiently to support an open circuit voltage. The cesium vapor is put into the generator section as a result of vaporizing liquid cesium. If the vaporizer does not boil cesium at a rate equal to the rate at which liquid cesium is injected into the boiler, then an accumulation of liquid in the vaporizer will result. The presence of such an accumulation can be ascertained by stopping the liquid flow and noticing if there remains an open circuit voltage measurement. If there is, then a monitoring of this voltage decay with respect to time can be used to determine a vaporizing rate of the cesium. From this rate a steady-state seed fraction level can be calculated. This experiment was performed and a calculated steady-state seed fraction of at least 0.001 can be achieved. This is comparable to the optimum fraction calculated in reference 2.

Curing the Loop

Two major sources of impurities exist in the loop: water and graphite. A castable refractory cement lines the heater, reheater, and the MHD duct. To cure the cement, the gas temperature is raised at a rate of 100 K per hour until 1200 K is attained. Then all the water, which is chemically and mechanically bonded to the refractory cement, is removed. However, it was impossible to attain 1200 K at every point in the heater refractory cement. Consequently, this cement is a continuing source of water vapor. The water, at these high temperatures, is decomposed by carbon into carbon monoxide and hydrogen. This reaction generates the major impurities monitored during the operation of the loop. The graphite heaters account for the second major source of gaseous impurities. Figure 15(a) shows the rapid generation of gaseous impurities at temperatures above 800 K. The loop required four purges in this first run to suppress the accumulation of hydrogen and other impurities. The dotted lines indicate an unknown impurity level immediately after a purge. Since the vacuum pumps reduce the loop pressure by a factor of 10^3, we assume a proportional reduction of the impurities. Figure 14(b) shows the data from run 5 which was taken after the facility had accumulated 70 hours of operation. Notice that at 2000 K the impurities are about a factor of three smaller than in run 1, and there were no purges in run 5.

Duct Insulation Resistance Measurements

At elevated temperatures and high contamination levels resistance between electrodes and ground is reduced. Figure 16 contains a sampling of data taken during run 5. At least four factors may contribute to the lower resistance measurements:

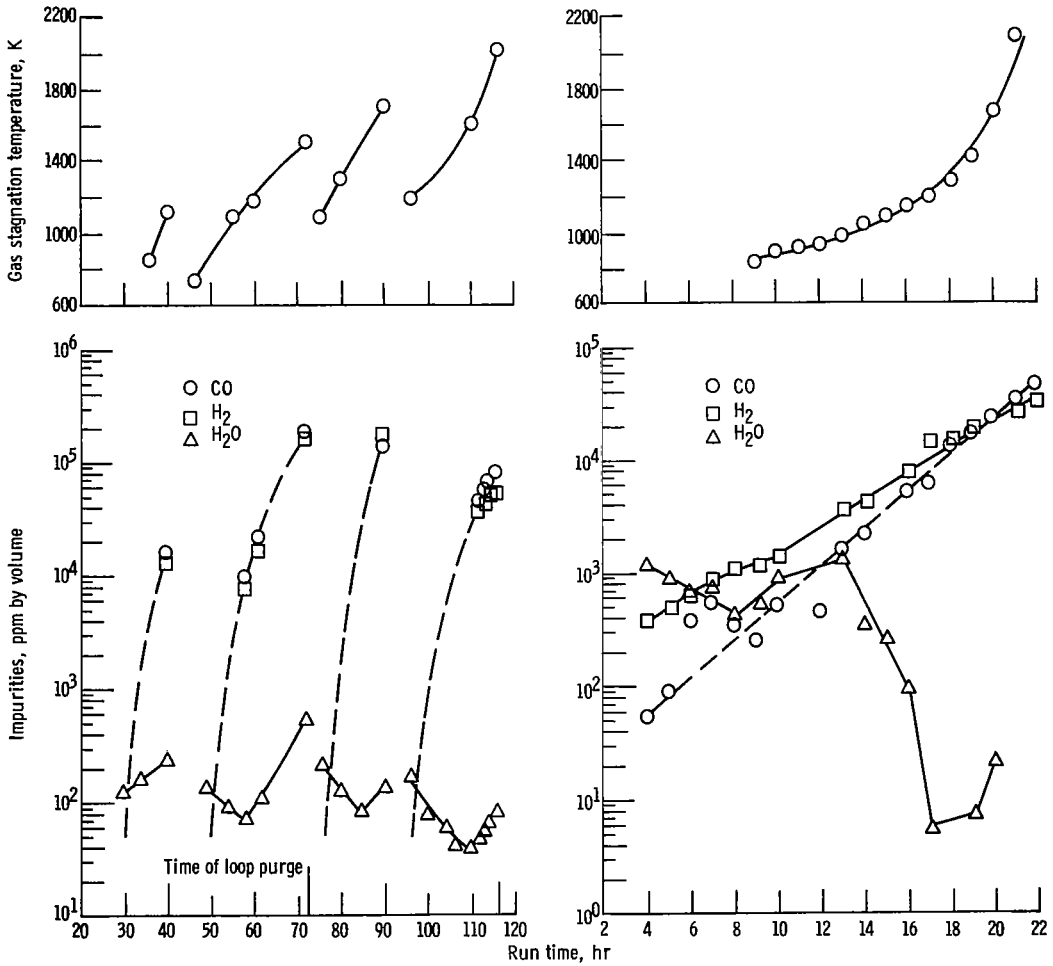

(a) Run 1. (b) Run 5.

Figure 15. - Impurities and temperature versus run time.

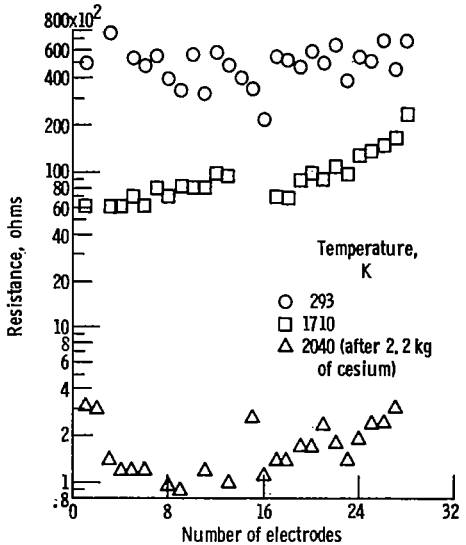

Figure 16. - Electrical resistance between generator cathodes and ground at several temperatures.

(1) The resistivity of the insulating brick and refractory cement decrease exponentially with increasing temperature. At 1900 K the resistivity of the brick is 10^4 ohm-centimeters compared with the resistivity at room temperature.

(2) Carbon may fill the voids in both the refractory brick and cement which insulate the duct.

(3) A carbon film may form on the ceramic insulator of each electrode feedthrough.

(4) Cesium may interact with the solid surfaces.

A combination of these factors contributes to the low-insulation resistance measured at 2040 K.

The low-temperature resistances (approximately 50 kilohms from each electrode to ground) are due to the voltmeter and cooling water, rather than the insulating material. The 1710 K temperature measurements appearing in figure 16 were taken before addition of cesium; the 2040 K data were taken several minutes after 2.2 kilograms of cesium was vaporized. Chemical analysis after run 5 showed that no cesium compounds existed on the surface of the high-density refractory brick. In addition, the electrode feedthroughs were examined and no cesium was found. Thus the effect of cesium on the resistance data taken at 2040 K is not clear. But in one particular case, while vaporizing cesium, the resistance between electrodes was monitored. The resistance fluctuated about zero - short circuit. This indicated that some interaction between the cesium and the insulating brick was taking place.

Further evidence indicating that leakage currents are an important factor in the present generator was found by measuring the open-circuit voltages. In the first set of runs, with a low seed fraction (0.0015) and no metallic support ribs, the open-circuit voltage across the duct was about 60 to 70 percent of the theoretical value. On the second set of runs, with a higher seed fraction (0.003) and the metallic ribs, the open-circuit voltage was about 30 percent of the theoretical value; and after about 2 kilograms of cesium were injected, this value was less than 20 percent. Thus, it appears that not only is there a degradation in the insulation to ground (fig. 16) but also between opposite electrodes. There is some indication that shorting across the duct may be the more severe limitation because the resistance can be smaller (i.e., nearly zero).

CONCLUDING REMARKS

The closed-loop, 2200 K MHD power generator facility has been quite successful in providing the necessary high-temperature working fluid, but the problems of generating MHD power efficiently in the facility are just being evaluated.

Lewis Research Center,
National Aeronautics and Space Administration,
Cleveland, Ohio, July 26, 1968,
129-02-01-07-22.

REFERENCES

1. IAEA/ENEA International Liaison Group on MHD Electrical Power Generation: Status Report on MHD Electrical Power Generation. Nucl. Fusion, vol. 7, no. 4, Dec. 1967, pp. 267-287.

2. Heighway, John E.; and Nichols, Lester D.: Brayton Cycle Magnetohydrodynamic Power Generation with Nonequilibrium Conductivity. NASA TN D-2651, 1965.

NASA-Langley, 1968 — 11 E-3884

NATIONAL AERONAUTICS AND SPACE ADMINISTRATION
WASHINGTON, D.C. 20546
OFFICIAL BUSINESS

FIRST CLASS MAIL

POSTAGE AND FEES PAID
NATIONAL AERONAUTICS AND
SPACE ADMINISTRATION

C2U 001 36 51 3DS 68285 00903
AIR FORCE WEAPONS LABORATORY/AFWL/
KIRTLAND AIR FORCE BASE, NEW MEXICO 8711

ATT E. LOU BOWMAN, ACTING CHIEF TECH. LI

POSTMASTER: If Undeliverable (Section 158 Postal Manual) Do Not Return

"The aeronautical and space activities of the United States shall be conducted so as to contribute . . . to the expansion of human knowledge of phenomena in the atmosphere and space. The Administration shall provide for the widest practicable and appropriate dissemination of information concerning its activities and the results thereof."

—NATIONAL AERONAUTICS AND SPACE ACT OF 1958

NASA SCIENTIFIC AND TECHNICAL PUBLICATIONS

TECHNICAL REPORTS: Scientific and technical information considered important, complete, and a lasting contribution to existing knowledge.

TECHNICAL NOTES: Information less broad in scope but nevertheless of importance as a contribution to existing knowledge.

TECHNICAL MEMORANDUMS: Information receiving limited distribution because of preliminary data, security classification, or other reasons.

CONTRACTOR REPORTS: Scientific and technical information generated under a NASA contract or grant and considered an important contribution to existing knowledge.

TECHNICAL TRANSLATIONS: Information published in a foreign language considered to merit NASA distribution in English.

SPECIAL PUBLICATIONS: Information derived from or of value to NASA activities. Publications include conference proceedings, monographs, data compilations, handbooks, sourcebooks, and special bibliographies.

TECHNOLOGY UTILIZATION PUBLICATIONS: Information on technology used by NASA that may be of particular interest in commercial and other non-aerospace applications. Publications include Tech Briefs, Technology Utilization Reports and Notes, and Technology Surveys.

Details on the availability of these publications may be obtained from:

SCIENTIFIC AND TECHNICAL INFORMATION DIVISION

NATIONAL AERONAUTICS AND SPACE ADMINISTRATION

Washington, D.C. 20546